Understanding the angle-independent photon harvesting in organic homo-tandem solar cells

Adrian Mertens, Jan Mescher, Daniel Bahro, Manuel Koppitz, and Alexander Colsmann*

Light Technology Institute, Karlsruhe Institute of Technology (KIT), Engesserstrasse 13, 76131 Karlsruhe, Germany

**alexander.colsmann@kit.edu*

Abstract: The effective device photo current of organic tandem solar cells is independent of the angle of light incidence up to 65°. This feature renders these devices particularly suitable for stationary applications where they receive mainly indirect light. In a combined experimental and simulative study, we develop a fundamental understanding of the causal absorption and charge generation mechanisms in organic homo-tandem solar cells. A 3-terminal tandem device architecture is used to measure the optoelectronic properties of both subcells individually. The analysis of the angle dependent external quantum efficiencies of the subcells and the tandem device reveal an internal balancing of the wavelength dependent subcell currents elucidating the low sensitivity of the tandem device properties on the angle of incidence.

OCIS codes: (310.6845) Thin film devices and applications; (250.0250) Optoelectronics; (350.6050) Solar energy; (160.4890) Organic materials; (160.4760) Optical properties.

References and links

1. G. Dennler, K. Forberich, M. C. Scharber, C. J. Brabec, I. Tomiš, K. Hingerl, and T. Fromherz, "Angle dependence of external and internal quantum efficiencies in bulk-heterojunction organic solar cells," J. Appl. Phys. **102**(5), 054516 (2007).
2. D. Cheyns, B. P. Rand, B. Verret, J. Genoe, J. Poortmans, and P. Heremans, "The angular response of ultrathin film organic solar cells," Appl. Phys. Lett. **92**(24), 243310 (2008).
3. A. Colsmann, J. Junge, C. Kayser, and U. Lemmer, "Organic tandem solar cells comprising polymer and small-molecule subcells," Appl. Phys. Lett. **89**(20), 203506 (2006).
4. J. Y. Kim, K. Lee, N. E. Coates, D. Moses, T. Q. Nguyen, M. Dante, and A. J. Heeger, "Efficient tandem polymer solar cells fabricated by all-solution processing," Science **317**(5835), 222–225 (2007).
5. G. Dennler, M. C. Scharber, T. Ameri, P. Denk, K. Forberich, C. Waldauf, and C. J. Brabec, "Design rules for donors in bulk-heterojunction tandem solar cells - towards 15% energy-conversion efficiency," Adv. Mater. **20**(3), 579–583 (2008).
6. V. S. Gevaerts, A. Furlan, M. M. Wienk, M. Turbiez, and R. A. J. Janssen, "Solution processed polymer tandem solar cell using efficient small and wide bandgap polymer:fullerene blends," Adv. Mater. **24**(16), 2130–2134 (2012).
7. B. E. Lassiter, J. D. Zimmerman, and S. R. Forrest, "Tandem organic photovoltaics incorporating two solution-processed small molecule donor layers," Appl. Phys. Lett. **103**(12), 123305 (2013).
8. B. Lechêne, G. Perrier, K. Emmanouil, S. Kennou, B. Bouthinon, and R. de Bettignies, "Design of intermediate layers for solution-processed tandem organic solar cells: guidelines from a case study on TiO_x and ZnO," Sol. Energy Mater. Sol. Cells **120**, 709–715 (2014).
9. A. Puetz, T. Stubhan, M. Reinhard, O. Loesch, E. Hammarberg, S. Wolf, C. Feldmann, H. Kalt, A. Colsmann, and U. Lemmer, "Organic solar cells incorporating buffer layers from indium zinc oxide nanoparticles," Sol. Energy Mater. Sol. Cells **95**(2), 579–585 (2011).
10. H. Zhou, Y. Zhang, C.-K. Mai, S. D. Collins, G. C. Bazan, T.-Q. Nguyen, and A. J. Heeger, "Polymer homo-tandem solar cells with best efficiency of 11.3%," Adv. Mater. **27**(10), 1767–1773 (2015).
11. J. You, C.-C. Chen, Z. Hong, K. Yoshimura, K. Ohya, R. Xu, S. Ye, J. Gao, G. Li, and Y. Yang, "10.2% power conversion efficiency polymer tandem solar cells consisting of two identical sub-cells," Adv. Mater. **25**(29), 3973–3978 (2013).
12. H. Kang, S. Kee, K. Yu, J. Lee, G. Kim, J. Kim, J.-R. Kim, J. Kong, and K. Lee, "Simplified tandem polymer solar cells with an ideal self-organized recombination layer," Adv. Mater. **27**(8), 1408–1413 (2015).

#257412 Received 14 Jan 2016; revised 23 Mar 2016; accepted 30 Mar 2016; published 22 Apr 2016

13. J. Gilot, M. M. Wienk, and R. A. J. Janssen, "Optimizing polymer tandem solar cells," Adv. Mater. **22**(8), E67–E71 (2010).
14. G. Dennler, K. Forberich, T. Ameri, C. Waldauf, P. Denk, C. J. Brabec, K. Hingerl, and A. J. Heeger, "Design of efficient organic tandem cells: on the interplay between molecular absorption and layer sequence," J. Appl. Phys. **102**(12), 123109 (2007).
15. A. Puetz, F. Steiner, J. Mescher, M. Reinhard, N. Christ, D. Kutsarov, H. Kalt, U. Lemmer, and A. Colsmann, "Solution processable, precursor based zinc oxide buffer layers for 4.5% efficient organic tandem solar cells," Org. Electron. **13**(11), 2696–2701 (2012).
16. J. Gilot, I. Barbu, M. M. Wienk, and R. A. J. Janssen, "The use of ZnO as optical spacer in polymer solar cells: Theoretical and experimental study," Appl. Phys. Lett. **91**(11), 113520 (2007).
17. F. Nickel, C. Sprau, M. F. G. Klein, P. Kapetana, N. Christ, X. Liu, S. Klinkhammer, U. Lemmer, and A. Colsmann, "Spatial mapping of photocurrents in organic solar cells comprising wedge-shaped absorber layers for an efficient material screening," Sol. Energy Mater. Sol. Cells **104**, 18–22 (2012).
18. C. Brabec, U. Scherf, and V. Dyakonov, *Organic Photovoltaics* (Wiley-VCH, 2014).
19. B. V. Andersson, U. Wuerfel, and O. Inganäs, "Full day modelling of V-shaped organic solar cell," Sol. Energy **85**(6), 1257–1263 (2011).
20. M. Riede, C. Uhrich, J. Widmer, R. Timmreck, D. Wynands, G. Schwartz, W.-M. Gnehr, D. Hildebrandt, A. Weiss, J. Hwang, S. Sundarraj, P. Erk, M. Pfeiffer, and K. Leo, "Efficient organic tandem solar cells based on small molecules," Adv. Funct. Mater. **21**(16), 3019–3028 (2011).
21. D. Bahro, M. Koppitz, A. Mertens, K. Glaser, J. Mescher, and A. Colsmann, "Understanding the external quantum efficiency of organic homo-tandem solar cells utilizing a three-terminal device architecture," Adv. Energy Mater. **5**(22), 1501019 (2015).
22. J. Gilot, M. M. Wienk, and R. A. J. Janssen, "Measuring the external quantum efficiency of two-terminal polymer tandem solar cells," Adv. Funct. Mater. **20**(22), 3904–3911 (2010).
23. N. Christ, S. W. Kettlitz, S. Züfle, S. Valouch, and U. Lemmer, "Nanosecond response of organic solar cells and photodiodes: Role of trap states," Phys. Rev. B **83**(19), 195211 (2011).
24. E. D. Palik, *Handbook of Optical Constants of Solids* (Academic Press, 1997).
25. A. Abdellaoui, G. Lévêque, A. Donnadieu, A. Bath, and B. Bouchikhi, "Iteratively derived optical constants of MoO_3 polycrystalline thin films prepared by CVD," Thin Solid Films **304**(1–2), 39–44 (1997).
26. R. Betancur, A. Martínez-Otero, X. Elias, P. Romero-Gómez, S. Colodrero, H. Miguez, and J. Martorell, "Optical interference for the matching of the external and internal quantum efficiencies in organic photovoltaic cells," Sol. Energy Mater. Sol. Cells **104**, 87–91 (2012).
27. M. Stolterfoht, B. Philippa, A. Armin, A. K. Pandey, R. D. White, P. L. Burn, P. Meredith, and A. Pivrikas, "Advantage of suppressed non-Langevin recombination in low mobility organic solar cells," Appl. Phys. Lett. **105**(1), 013302 (2014).
28. J. Yang, R. Zhu, Z. Hong, Y. He, A. Kumar, Y. Li, and Y. Yang, "A robust inter-connecting layer for achieving high performance tandem polymer solar cells," Adv. Mater. **23**(30), 3465–3470 (2011).

1. Introduction

The exceptionally good absorption of diffuse light is one of the most promoted properties of organic solar cells, giving advantage over other mature photovoltaic technologies [1,2]. In case of facade or window integration, which are commonly considered key applications for organic photovoltaics, sun tracking is impossible, rendering the angle-dependent light absorption properties of solar cells very important. As the field of organic photovoltaics progresses, new concepts for yielding higher power conversion efficiencies (PCEs) are developed. A promising concept to increase the PCE of organic solar cells is the tandem device architecture that incorporates two monolithically stacked and electrically interconnected solar cells [3–7]. By incorporating two spectrally complementary absorbers into the tandem device, a better coverage of the solar spectrum can be achieved. Utilizing twice the same absorber (homo-tandem solar cell) can compensate moderate optical densities of absorbers, account for moderate charge carrier mobilities by reducing the active layer thickness, or reduce the device current while providing higher device voltages [8,9]. The latter is particularly beneficial for large-area solar modules where the lateral series resistance of electrodes requires special attention. Organic homo-tandem solar cells with PCEs exceeding 10% have been reported in the literature [10–12]. So far, the maximum PCE in tandem solar cells has been achieved when the photo currents of both subcells have been matched, although, in non-matched devices, the stronger subcell may assist the weaker subcell with the extraction of charges [13]. The matching of photo currents very much depends on the optical field in the tandem device and hence the charge carrier generation profile [14,15]. Organic

#257412 Received 14 Jan 2016; revised 23 Mar 2016; accepted 30 Mar 2016; published 22 Apr 2016

tandem devices comprise several thin layers with thicknesses on the order of the wavelength of the incident sunlight. Hence, the optical field distribution within the layer stack and, consequently, the charge carrier generation profile are dominated by thin-film interferences which depend on the thicknesses and the complex refractive indices of the various layers [16–18]. As a consequence, intuitively, one would expect a strong susceptibility of the tandem solar cells' photo currents to the angle of light incidence due to its advanced thin-film device architecture [2,19]. Surprisingly, in organic tandem solar cells comprising molecular absorber layers, the photo current generation was reported to be angle-independent, with the question remaining why the integrated absorption profiles of the subcells are mostly unaffected by the angle of illumination [20]. In this work, we develop a detailed understanding of the spectral photo-generation of charge carriers in the subscells of polymer homo-tandem solar cells by combining simulation and experiment. For the latter, we fabricated organic tandem solar cells that employ a recombination zone from poly(3,4-ethylenedioxythiophene):polystyrene sulfonate and zinc oxide (PEDOT:PSS/ZnO), according to the inverted device architecture depicted in Fig. 1(a). As a special feature, the tandem solar cells are designed to equally operate in 2-terminal and 3-terminal mode, *i.e.*, they comprise an intermediate transparent electrode to enable separate characterization of the subcells and hence to yield a better understanding of the absorption within the device. This intermediate transparent electrode was realized by utilizing highly conductive PEDOT:PSS [21].

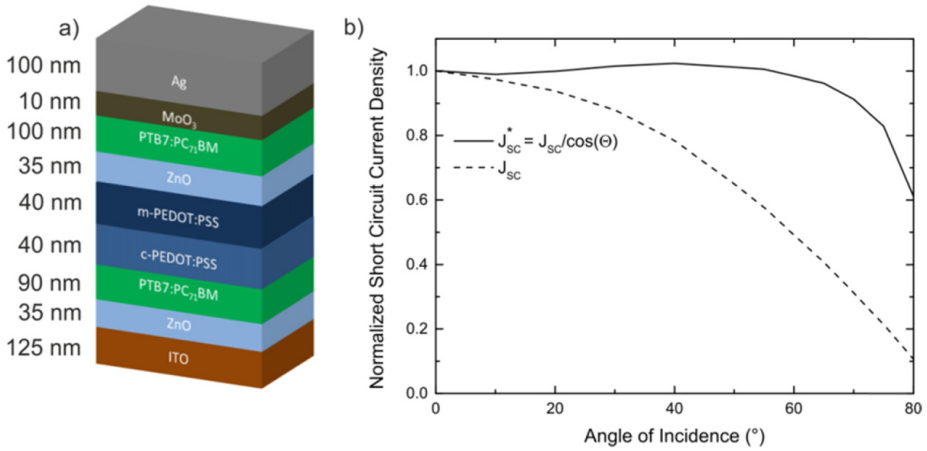

Fig. 1. (a) Tandem solar cell device architecture comprising a PEDOT:PSS/ZnO recombination zone. The PEDOT:PSS layer was partly realized from conductive PEDOT:PSS to give access to the subcells. (b) Short circuit current density J_{SC} of the tandem device versus the angle of light incidence. To account for the change of the effective solar cell size under oblique illumination, the photo current was divided by cos(θ). The tandem device generates an almost constant effective photo current $J^*_{SC}(\theta)$ up to angles of incidence θ of about 65°.

2. Results and discussion

The 3-terminal architecture enables both the characterization of the tandem solar cell in the common 2-terminal mode by measuring the J-V curve between the outer electrodes and the characterization of the individual subcells by utilizing the intermediate contact (3-terminal mode). A typical 3-terminal tandem device exhibits a short circuit current density J_{SC} = 7.5 mA/cm^2 and a fill factor of FF = 65% when measured in 2-terminal mode under normal light incidence. The open circuit voltages of the subcells add up to V_{OC} = 1430 mV, resulting in an overall PCE = 7%.

Figure 1(b) depicts the normalized photo current density of a typical 3-terminal tandem solar cell measured in 2-terminal mode versus the angle of light incidence (dashed line). To account for the change of the effective area under angular illumination, we henceforth

#257412 Received 14 Jan 2016; revised 23 Mar 2016; accepted 30 Mar 2016; published 22 Apr 2016

multiply the photo current densities with 1/cos(θ) (solid line) where θ represents the angle of incidence, *i.e.*, the angle between the incident light and the sample surface normal. The curves are thus normalized to the reduced radiant flux density and represent an effective photo current density. For angles θ < 20°, the effective short circuit current density $J^*_{SC}(\theta)$ remains about constant. Interestingly, for angles 20° < θ < 60°, $J^*_{SC}(\theta)$ slightly increases as compared to the short circuit current density $J^*_{SC}(0)$ at normal incidence. Again, this observation appears counterintuitive for tandem devices that strongly depend on current matching in the subcells. The current matching is coupled to the spatial absorption profile and hence the thin-film interference patterns that in turn depend on the angle of incidence. To understand the optoelectronic origins of this widely angle-independent photo current generation of the tandem device, we characterized the tandem solar cell in 3-terminal mode by utilizing the transparent intermediate PEDOT:PSS electrode that gives access to the optoelectronic properties of the two subcells.

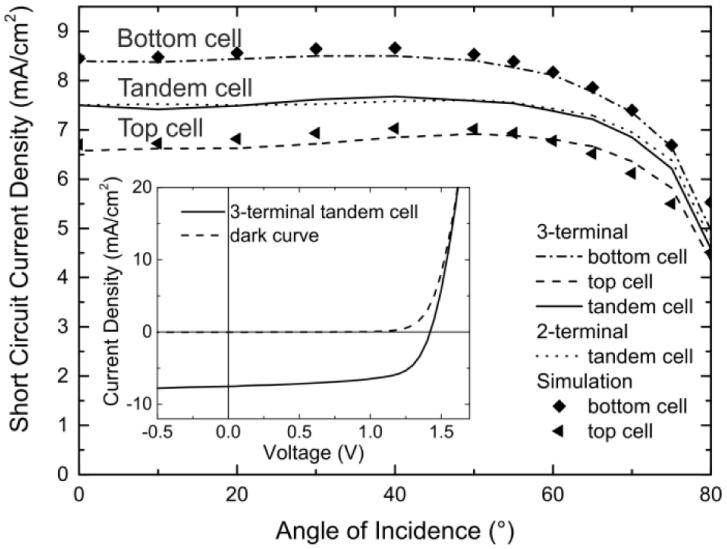

Fig. 2. Measured $J^*_{SC}(\theta)$ of a typical 3-terminal tandem device (solid line), a 2-terminal reference device (dotted line), the bottom subcell of the 3-terminal tandem solar cell (dashed-dotted line) and the respective top subcell (dashed lines) versus the angle of light incidence. The squares and the triangles represent the corresponding results of the optical simulation of the two subcells. Inset: The corresponding J-V curve of the 3-terminal tandem device.

In Fig. 2, the dashed line and the dashed-dotted line represent the angle-dependent photo currents of the bottom and the top subcells measured between the intermediate PEDOT:PSS electrode and the respective outer electrode, in comparison to the photo current $J^*_{SC}(\theta)$ of the tandem device (solid line). Both subcells show the same dependence of J^*_{SC} on the angle of incidence θ with the bottom cell performing somewhat better than the top cell. We note that the subcell currents are slightly mismatched and that the excess of generated charge carriers in the bottom cell at all angles leads to an electric field across the top cell, assisting the extraction of charges from the top cell. Therefore, the tandem device is not limited by the weaker cell but rather delivers an intermediate photo current as described in literature before [22]. We note that we have deliberately chosen a layer architecture with mismatched subcell J^*_{SC}'s in order to show the universality of the approach as tandem solar cells in real-life applications will rarely exhibit matched photo currents due to frequent changes of the incident light spectrum in the course of a day. We found confirmation of our experimental results in optical simulations based on the transfer matrix method [23]. All optical simulations were performed under virtual AM1.5 illumination. The refractive indices of ITO, ZnO,

#257412 Received 14 Jan 2016; revised 23 Mar 2016; accepted 30 Mar 2016; published 22 Apr 2016

PEDOT:PSS and PTB7:$PC_{71}BM$ were determined by spectroscopic ellipsometry. The complex refractive indices of MoO_3 and Ag were taken from literature [24,25].

The squares (bottom cell) and the triangles (top cell) in Fig. 2 show the angle dependent $J^*_{SC}(\theta)$ of the subcells obtained by optical simulation using an overall internal quantum efficiency (IQE) of 88% [26] to match the device short circuit current density. We note that a spectrally resolved simulation would require to take the wavelength dependent IQE into account (not required here) [27]. The shapes of the experimental and simulated results show very good agreement. Hence we conclude that both subcells and the tandem solar cell generate about constant $J^*_{SC}(\theta)$ for all angles θ up to 65°.The constant photo currents in the tandem device for $\theta < 65°$ are particularly surprising since a variation of the incident angle leads to changes of the optical path of the light within the device and the reflection and transmission properties at each interface. Thus, one would expect that the concomitant change of the optical field affects the subcell absorption. A better understanding of the subcell absorption can be gained from more detailed optical device simulations. Figure 3 illustrates the spatially resolved absorption profile throughout the 3-terminal device for angles of incidence θ up to 85°. The simulation results are exemplified for the incident light wavelengths $\lambda_1 = 470$ nm (Fig. 3(a)) and $\lambda_2 = 700$ nm (Fig. 3(b)) but can be discussed for any other wavelength likewise. For both wavelengths, at an angle of incidence $\theta = 0°$, we find the first spatial absorption maximum (constructive interference) close to the metal anode and within the top absorber layer. Further away from the anode, in the bottom absorber layer, the 470 nm light has a spatial minimum (destructive interference) while the 700 nm light shows a second maximum.

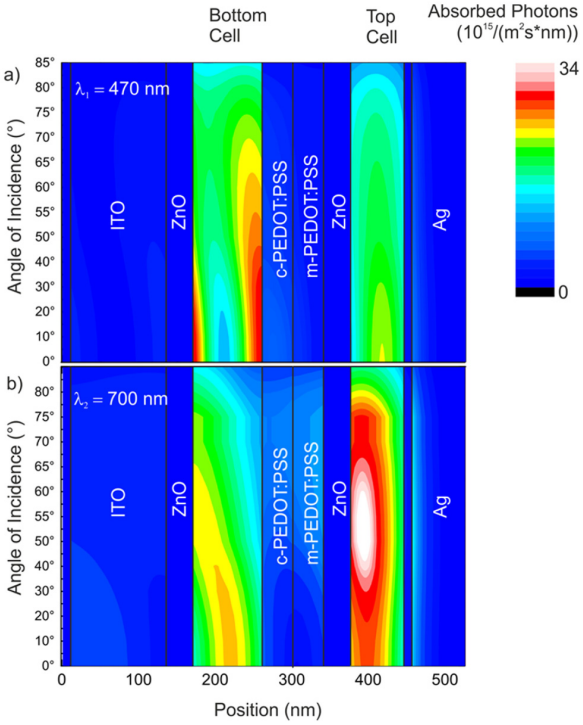

Fig. 3. Spatially resolved absorption profiles of the 3-terminal devices for angles of incidence up to 85° for (a) 470 nm and (b) 700 nm incident wavelengths. While the optical field in the top cell is almost unaffected by the angle of incidence, we observe a significant shift of the absorption profile away from the anode in the bottom subcell. For 700 nm the shift of the maxima inside the absorber layer is more pronounced than for 470 nm, which leads to a blue shift of the absorption and hence the EQE. The angle dependent absorption of the two subcells is in good agreement with the measured EQEs.

#257412 Received 14 Jan 2016; revised 23 Mar 2016; accepted 30 Mar 2016; published 22 Apr 2016

Upon increasing the angle of incidence θ, all maxima and minima are successively shifted away from the anode. Whereas this effect is less significant in the top subcell, it becomes more pronounced in the bottom subcell due to the longer distance from the metal electrode. We therefore expect a wavelength dependent modulation of the subcell EQE, being more prominent in the bottom subcell than in the top subcell. Accordingly, we experimentally investigated the angle dependent EQEs of both subcells to study the influence of the angle of incidence on the subcell properties and the angle dependent photo current generation in the tandem device. As depicted in Fig. 4(a), under normal incidence (θ = 0°), the EQE of the PTB7:$PC_{71}BM$ top cell exhibits absorption peaks at 450 nm ($PC_{71}BM$) as well as 670 nm and 720 nm (PTB7). Towards small increasing angles of incidence θ, the EQE does not show any significant changes. For intermediate angles (θ ≈50°), the absorption peaks broaden, thereby slightly increasing the total absorption of the device which is in excellent accordance with the observed $J^*_{SC}(\theta)$ increase in the top cell. We note that for technical reasons, we did not use any white bias light for the angle dependent EQE measurement, which results in a slight overestimation of the EQE and the calculated $J^*_{SC}(\theta)$, respectively, but does not change the interpretation of the results [18]. For high angles of incidence θ, we find an almost flat EQE spectrum. This flattening of the EQE can be attributed to a longer propagation path of the incident light through the absorber layer and therefore a more homogeneous absorption of light throughout the visible spectrum. The overall reduction of the EQE towards higher θ originates from enhanced reflection at the device surface for grazing light incidence. For the bottom solar cell, we observe a similar broadening of the EQE spectrum towards increasing angles of incidence θ in Fig. 4(b). Due to the longer distance from the metal electrode and hence a more pronounced spatial shift of the thin-film interferences in the absorber layer towards higher angles of incidence, we observe a stronger spectral modulation of the EQE. In contrast to the top cell, the EQE of the bottom cell decreases in the long-wavelength regime, while the EQE in the short-wavelength regime is increased, both nicely reflecting the simulated shift of interference peaks as discussed above and depicted in Fig. 3. However, the $J^*_{SC}(\theta)$ of the subcells and the tandem devices is hardly affected by this EQE modulation: as depicted in the insets of Figs. 4(a) and 4(b), integration of the EQE yields the same $J^*_{SC}(\theta)$ profile as compared to the direct measurement of the subcells' $J^*_{SC}(\theta)$ via the intermediate electrode.

In order to demonstrate the portability of all considerations presented herein to the more common 2-terminal device architecture without a conductive intermediate contact, we also fabricated 2-terminal homo-tandem solar cells with equal optoelectronic properties, where the 80 nm PEDOT:PSS layer in the recombination zone was entirely fabricated from non-conductive m-PEDOT:PSS. The respective J-V curves are congruent and all key performance data are equal. Moreover, as depicted in Fig. 2, the angle dependent $J^*_{SC}(\theta)$ of this 2-terminal device (dotted line) and the 3-terminal tandem solar cell (solid line) match well within the measurement certainty. We note that we have observed similar angle-dependency of the photo currents in various other homo- and hetero-tandem solar cells (data not shown here).

In conclusion, the about constant effective photo current of organic homo-tandem solar cells under illumination at angles of incidence up to 65° can be attributed to a shift of the wavelength dependent charge carrier generation profile. Although the charge carrier generation profile depends on the wavelength of the incident light under oblique angles, the integrated number of photo-generated charges remains constant due to the mutual compensation of charges generated at different wavelengths and the field-assisted extraction of charges from the weaker subcell by the charge carrier excess generated by the stronger subcell. This property renders organic tandem solar cells suitable to harvest indirect sunlight or oblique direct sunlight in stationary applications, equally to their single-junction counterparts.

#257412 Received 14 Jan 2016; revised 23 Mar 2016; accepted 30 Mar 2016; published 22 Apr 2016

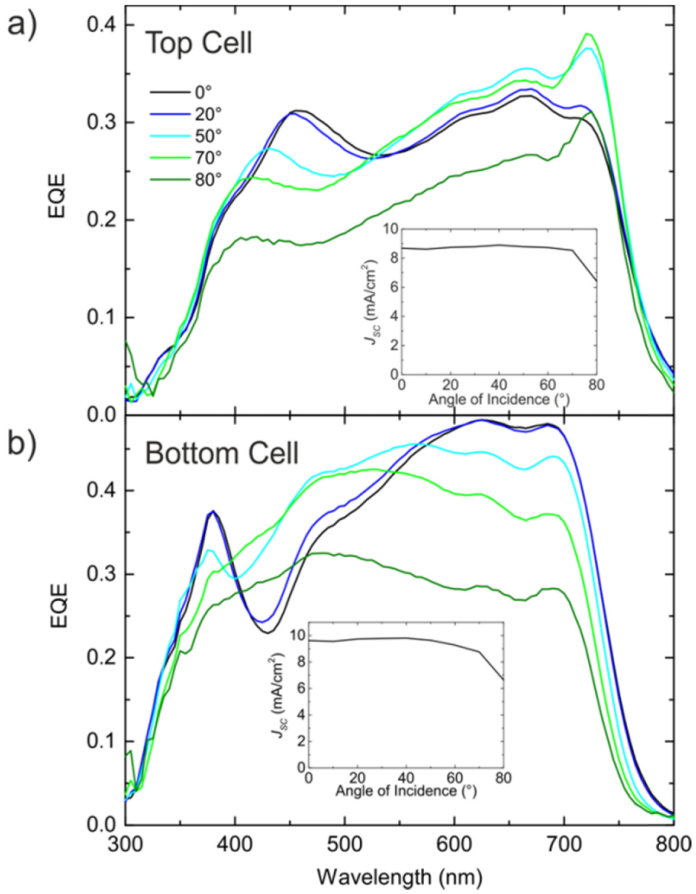

Fig. 4. The angle dependent EQEs of (a) the top subcell and (b) the bottom subcell. With increasing angle of light incidence, the EQE spectra flatten. Despite of the significant wavelength-dependent changes in the EQE for different angles of incidence, the angle-dependent integrated EQE is in good agreement with the angle-dependent $J^*_{SC}(\theta)$ measurements in Fig. 2. The respective simulated EQEs are provided in the Appendix, Figs. 5(c) and 5(d).

3. Experiment

All devices were fabricated at room temperature on indium tin oxide (ITO) coated glass substrates (d_{ITO} = 125 nm, $R_{\square}$ ≈13 Ω/sq) which were structured in hydrochloric acid and subsequently cleaned with acetone (15 min) and isopropanol (15 min) in an ultrasonic bath. Zinc oxide nanoparticles (ZnO, Nanograde Ltd.) were spin cast from dispersion (1 wt% IPA, 4000 rpm, 30 sec) and then annealed (80 °C, 10 min), forming a layer with a thickness of 35 nm. For both active layers, poly({4,8-bis[(2-ethylhexyl)oxy]benzo[1,2-b:4,5-b`]dithiophene-2,6-diyl}{3-fluoro-2-[(2-ethylhexyl)carbonyl]thieno[3,4-b]thiophenediyl} (PTB7, 1-Material Inc., M_w = 125 kg/mol, $Đ_M$ = 2.5) and [6,6]-phenyl C_{71}-butyric acid methyl ester ($PC_{71}BM$, Sigma Aldrich) were dissolved separately in chlorobenzene (25 mg/mL) and then mixed at a ratio of 2:3. Then 4 vol% 1,8-diiodooctane were added. The solutions were spun onto the substrate (2000 rpm, 60 sec) to yield photo active layers with thicknesses of 90 nm for the bottom cell and 100 nm (1500 rpm, 60 sec) for the top cell. Afterwards, the samples were annealed at 60 °C for 20 minutes. The recombination zone comprised an 80 nm thick PEDOT:PSS layer for hole extraction from the bottom cell and a 35 nm thick ZnO nanoparticle layer for electron extraction from the top cell. The 80 nm PEDOT:PSS layer

#257412 Received 14 Jan 2016; revised 23 Mar 2016; accepted 30 Mar 2016; published 22 Apr 2016

itself, comprises two sublayers with different functionality. To access the individual subcells of the homo tandem device, the first 40 nm sublayer was deposited from conductive PEDOT:PSS (c-PEDOT:PSS, Clevios FHC Solar, Heraeus) which acts as a conductive intermediate contact. The second 40 nm sublayer (Clevios HTL Solar, Heraeus) was modified (m-PEDOT:PSS) by sodium polystyrene sulfonate (SPS 100 g/L H_2O, 4 vol%) to provide a solvent barrier and hence protection of the bottom cell during the application of the top solar cell [28]. 10 nm molybdenum oxide (MoO_3, Sigma Aldrich) and a silver (Ag) back contact (100 nm) were thermally evaporated on top of the device. The cross-section of all electrodes defined the photo-active area of the solar cell (A_{active} = 10.5 mm^2). All devices were characterized under AM1.5G illumination (100 mW/cm^2) from a spectrally monitored Oriel 300 W solar simulator. Current density-voltage (J-V) curves were recorded with a Keithley 238 source measure unit. External quantum efficiency (EQE) measurements were performed on an in-house built system comprising a xenon lamp, a LOT-Oriel Omni Lambda 300 monochromator, an Anfatec eLockIn 204/2 and a calibrated photodiode from Thorlabs [22]. For the angle dependent measurements, a modified PI-Instruments rotation stage (C-863.11 Mercury) was used.

Appendix

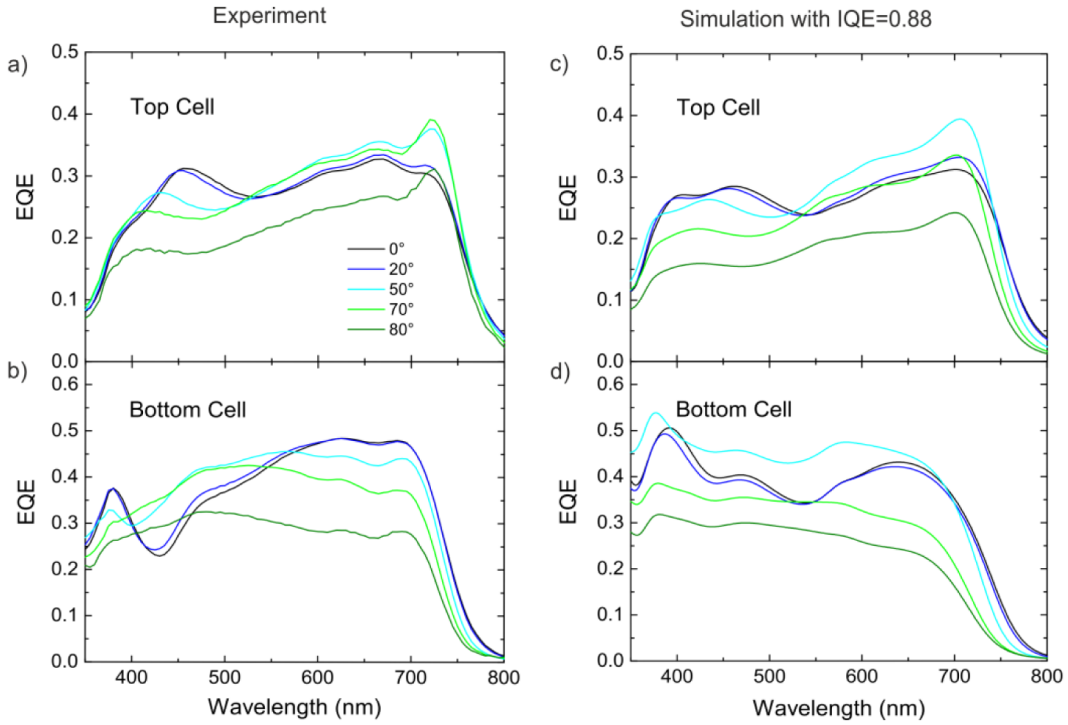

Fig. 5. The angle dependent EQEs of (a) the top subcell and (b) the bottom subcell in comparison with the optical simulation (c) and (d). The simulation differs from the measurements due to minor deviations of the actual layer thicknesses in the tandem devices. We note that the overestimation of the simulated EQEs for small wavelengths originates from the spectrally flat IQE that was assumed here. Earlier investigations of PTB7:$PC_{71}BM$ have demonstrated a slightly wavelength dependent IQE, which is below 0.88 for wavelengths $\lambda <$ 500 nm [27]. Still, the qualitative trends of both, simulation and experiment, are in well accordance.

#257412 Received 14 Jan 2016; revised 23 Mar 2016; accepted 30 Mar 2016; published 22 Apr 2016

Acknowledgments

A. Mertens and J. Mescher contributed equally to this work. We thank Uli Lemmer for fruitful discussions and Nanograde Ltd. for providing ZnO nanoparticles. This work was funded by the Federal Ministry of Education and Research under contract 03EK3504 (project TAURUS). A. Mertens and J. Mescher acknowledge support by the Karlsruhe School of Optics & Photonics (KSOP). We acknowledge support by Deutsche Forschungsgemeinschaft and Open Access Publishing Fund of Karlsruhe Institute of Technology.

#257412 Received 14 Jan 2016; revised 23 Mar 2016; accepted 30 Mar 2016; published 22 Apr 2016